



Analytical stability study for a densification front in a Carbon/Carbon composite

Gerard L. Vignoles, Roland Duclous, Simon Gaillard

► To cite this version:

Gerard L. Vignoles, Roland Duclous, Simon Gaillard. Analytical stability study for a densification front in a Carbon/Carbon composite. Chemical Engineering Science, 2007, 62, pp.6081- 6089. <10.1016/j.ces.2007.06.022>. <hal-00407506>

HAL Id: hal-00407506

<https://hal.science/hal-00407506v1>

Submitted on 9 Sep 2023

HAL is a multi-disciplinary open access archive for the deposit and dissemination of scientific research documents, whether they are published or not. The documents may come from teaching and research institutions in France or abroad, or from public or private research centers.

L'archive ouverte pluridisciplinaire **HAL**, est destinée au dépôt et à la diffusion de documents scientifiques de niveau recherche, publiés ou non, émanant des établissements d'enseignement et de recherche français ou étrangers, des laboratoires publics ou privés.



Distributed under a Creative Commons CC BY-NC-ND 4.0 - Attribution - Non-commercial use - No Derivative Works - International License

Author's Accepted Manuscript

Analytical stability study of the densification front in carbon- or ceramic-matrix composites processing by TG-CVI

Gérard L. Vignoles, Roland Ducloux, Simon Gaillard

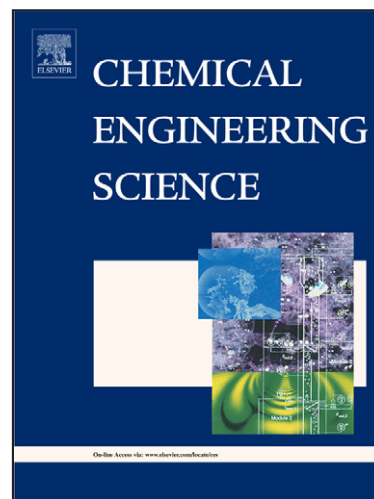
PII: S0009-2509(07)00472-1
DOI: doi:10.1016/j.ces.2007.06.022
Reference: CES 7491

To appear in: *Chemical Engineering Science*

Received date: 14 November 2006
Revised date: 24 May 2007
Accepted date: 11 June 2007

Cite this article as: Gérard L. Vignoles, Roland Ducloux and Simon Gaillard, Analytical stability study of the densification front in carbon- or ceramic-matrix composites processing by TG-CVI, *Chemical Engineering Science* (2007), doi:10.1016/j.ces.2007.06.022

This is a PDF file of an unedited manuscript that has been accepted for publication. As a service to our customers we are providing this early version of the manuscript. The manuscript will undergo copyediting, typesetting, and review of the resulting galley proof before it is published in its final citable form. Please note that during the production process errors may be discovered which could affect the content, and all legal disclaimers that apply to the journal pertain.



www.elsevier.com/locate/ces

Analytical stability study of the densification front in carbon- or ceramic-matrix composites processing by TG-CVI

G rard L. Vignoles ^{*}, Roland Duclous ¹, Simon Gaillard ²

Laboratoire des Composites ThermoStructuraux (LCTS), UMR 5801

*CNRS-CEA-Safran-Universit  Bordeaux I, 3, All e La Bo tie, F-33600 Pessac,
France*

Abstract

Thermal-Gradient Chemical Vapor Infiltration (TG-CVI) is a group of alternatives to classical CVI, involving a strong thermal gradient. It allows one to fabricate *e. g.* carbon-matrix or ceramic-matrix composite materials starting from a fibrous preform and a gaseous precursor, the cracking of which results in a solid deposit constituting the composite matrix. The main interest of these processes is a short fabrication time; however, their control is difficult. Past modelling works [Vignoles et al.(2006), Nadeau et al.(2006)] have shown that process control and optimization are possible and are based on the notion of densification front. In this paper, a 2D transverse stability study is presented for this front. A condition for stability is worked out; the influence of processing parameters is discussed. It appears that in usual processing cases, the stability criterion is fulfilled, but that it could be violated if some careless process up-scaling is performed.

¹ currently at Center for Studies on Intense Lasers and Applications (CELIA), UMR 5107 CNRS-CEA-Univ. Bordeaux 1, 351 Cours de la Lib ration, F33405 Talence, France

² currently at Matmeca Engineering School, Univ. Bordeaux 1, 351 Cours de la Lib ration, F33405 Talence, France

Key words: Composites, Materials Processing, Modelling, Porous media, Process stability

Accepted manuscript

1 Introduction

Chemical Vapor Infiltration is one of the main routes for the processing of carbon and ceramic matrices in thermostructural composites [Naslain and Langlais(1990), Besmann et al.(1991)]. Its principle rests on the heterogeneous deposition reaction of a gaseous precursor inside the preform, a porous medium constituted by fiber felts or woven fabrics which are intended to reinforce the future material. The first implementations of CVI – still in use today – were carried out in isothermal conditions. It has been shown experimentally and theoretically [Middleman(1989), Chung et al.(1991), Fédou et al.(1993), Sotirchos(1991)] that isothermal CVI (I-CVI) involves the competition between gas diffusion and reaction. A straightforward Thiele modulus analysis implies then that moderate temperature and low pressure are adequate conditions to avoid premature pore plugging and thus to preserve the material quality, in terms of matrix deposition homogeneity [Reuge and Vignoles(2005)]. The drawback of such conditions is that the chemical kinetics are dramatically slow, turning I-CVI a very lengthy and expensive process.

A variety of CVI modifications have then been designed in order to overcome this limitation. We refer the interested reader to the exhaustive review of [Golecki(1997)] for a discussion of all modifications. Most of them rely on the use of a thermal gradient, because this can help controlling the chemical reaction and make it happen at the right place first – that is, at the center of the preform, or at its borders which lie farthest from the impinging gas

* to whom correspondence should be addressed

Email addresses: `vinhola@lcts.u-bordeaux1.fr` (Gérard L. Vignoles),
`duclos@celia.u-bordeaux1.fr` (Roland Duclous),
`simon.gaillard@etu.u-bordeaux1.fr` (Simon Gaillard).

flux [Gupte and Tsamopoulos(1989), Melkote and Jensen(1990)].

The forced CVI (F-CVI) process was initially based on the intent of accelerating chemical deposition by forcing the gases through the pores with a pressure drop [Besmann et al.(1991), Vaidyaraman et al.(1995), Besmann and McLaughlin(1994), Starr et al.(1991)], but it has been rapidly found out that the superposition of a thermal gradient would enhance the quality and processing time. Golecki *et al.* have implemented a "rapid densification" process [Golecki et al.(1994)] based on isobaric conditions and the creation of a "hot side" and "cold side" on the preforms. Impeding the gas entrance by the hot side helps in densifying the pore bottom at first and the pore mouth at last, as wanted. In practice, one uses a central inductor or resistor around which the preforms are settled. Thermal-gradient isobaric CVI (TG-CVI) has also been considered with in-situ heat production, like microwave heating (MW-CVI) [Gupta and Evans(1991), Morell et al.(1992), Devlin et al.(1992)] or radio-frequency induction heating (RF-CVI) [Devlin et al.(1996), Midha and Economou(1997), Leutard et al.(2002)], with the idea of creating a hot deposition zone directly at the preform center. Houdayer *et al.* [Houdayer et al.(1984)] have implemented a "film-boiling" process, also called Kalamazoo, which consists in having the preform, heated as in the preceding processes, merged into boiling precursor. This helps one to maintain its surface temperature at a constant, well-known value, and ensure a very strong thermal gradient [Bruneton et al.(1997)]. All these CVI modifications have the advantage of allowing one to work with higher pressures, higher temperatures, and consequently higher rates and lower processing times.

Recent modelling advances on the isobaric modifications of TG-CVI [Leutard et al.(2002), Lines et al.(2005), Vignoles et al.(2006), Vignoles et al.(2005), Nadeau et al.(2006)] have emphasized the key role played by the densification front. Indeed, when this front exists, a quite complete infiltration may be performed in a single run, and in shorter processing times than in I-CVI. The

existence of the front is subject to a criterion which translates the fact that diffusion has to be fast enough through the front itself (its width being dictated by the thermal gradient) to feed properly the deposition reaction inside it. The front characteristic quantities : width, velocity, and residual porosity left behind it, have been related to the experimental and preform parameters [Nadeau et al.(2006)]. One important issue has been left out so far : the stability of the front. This is the aim of the present contribution.

The first part of this paper will briefly recall the description of the TG-CVI processes and of the densification front. Balance equations will be written for heat, precursor gas and solid mass, at a local scale linked to the front itself, and at a larger scale. Then, an analytical stability study will be performed, leading to a dispersion relation. Finally, using this relation, the influence of process and material parameters on the front stability will be discussed.

2 CVI with thermal gradients

CVI processes involve the introduction of a precursor gas inside a porous preform. When temperature is high enough, this gas reacts with the preform : solid deposition then occurs and the pores are progressively plugged. When one part of the preform is maintained at a higher temperature, reaction occurs mainly there, because of the extreme sensitivity of reaction kinetics to temperature. All that has to be done is to feed the reaction zone by bringing gas from the raw, non-infiltrated side.

Mass and heat transport are the principal identified phenomena, together with deposition. Both take place in the porous medium:

- Mass transport (gas phase) is mainly due to a reactant gas concentration gradient. Except in the F-CVI modification, which involves high pressure gradients, the resulting flow is mostly diffusive.

- On the other hand, heat transport mainly occurs through the solid phase, by conduction. This is because thermal conductivity is much lower in the gas phase than in the solid phase.

During deposition, the porosity decreases until a percolation threshold is reached. Its value may be fairly low in "film-boiling" experiments. In a typical run with cylindrical symmetry and inner heating, the following steps occur (see fig.1) :

- (1) The center of the preform is heated by contact with a carbon resistor or susceptor. Its outer boundary is in contact with cool precursor gas. It also loses heat by radiation, conduction, and possibly convection. In the film-boiling modification, the existence of a biphasic zone outside the preform guarantees that its outer side temperature is close to the precursor boiling point.
- (2) As soon as a sufficient temperature is attained, solid deposition will occur. The infiltration area, first located at the inner boundary, moves towards the exterior. As a consequence, the infiltrated part is not an obstacle for the mass flux, which settles from the outside to the inside, in order to counter-balance the precursor consumption in the front.
- (3) The infiltrated zone has a high thermal conductivity, as compared to the raw preform : consequently, the thermal gradient is pushed outside this zone and stays in the remaining raw preform zone.

3 Local front results

Some results derived in [Nadeau et al.(2006)] are recalled in order to introduce variables required for the stability study. After pore-scale averaging, the heterogeneous deposition rate obeys the following expression :

$$R = \sigma_v \cdot k(T) \cdot C \quad (1)$$

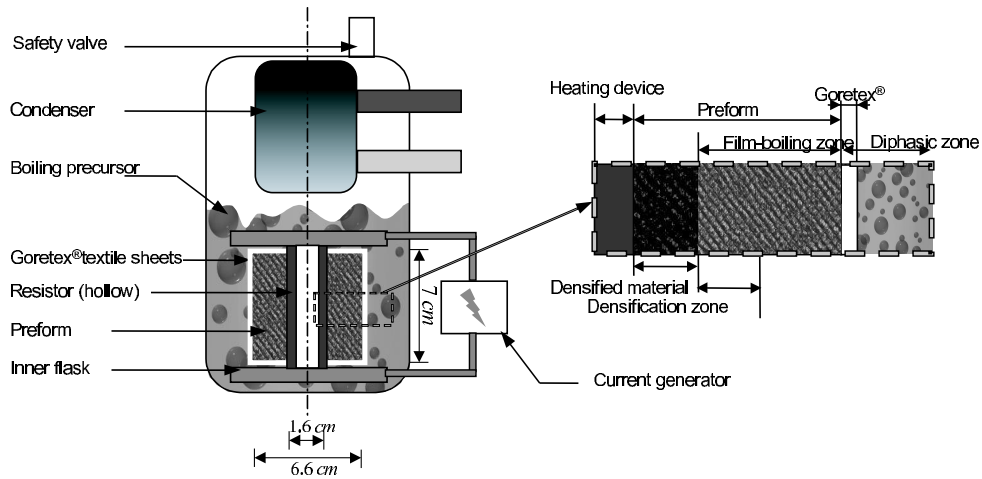


Fig. 1. Descriptive scheme of the film-boiling CVI process.

where $k(T)$ is given by an Arrhenius law :

$$k(T) = k_0 \exp \left(-\frac{E_a}{RT} \right) \quad (2)$$

From these relations it is seen that deposition depends on:

- The *accessible* gas/solid interface area $\sigma_v(\varepsilon)$, ε being the *open* porosity.
- The precursor gas concentration C
- The temperature T through the chemical reaction constant.

As a consequence, the reaction occurs only where $R(x, z, t) > 0$: this provides criteria for defining the front boundaries.

- $k(T) > 0$: There is a need for a minimum (ignition) temperature: T_i . The "cold" boundary is defined by $T(x, z) = T_i$.
- $\sigma_v(\varepsilon(x, z)) = 0$ defines a "total densification" boundary.
- $C(x, z) = 0$ defines a "reactant depletion" boundary.

The last two conditions are rarely met together; however one of them suffices to define a "hot" boundary. As a consequence, two kinds of front may occur. Whether one or the other occurs depends on the precise functional dependen-

cies of $\sigma_v(\varepsilon)$ and $D(\varepsilon)$. In practice, only the second type of front occurs, *i.e.* a reactant depletion front, that displays some residual open porosity. Indeed, it has been shown [Nadeau et al.(2006)] that a criterion for a total densification front is : $m + 1/n < 1$, where $m = \frac{\partial \ln D}{\partial \ln \varepsilon} - 1$ is a translation of the notion of tortuosity and $n = \left(\frac{\partial \ln \sigma_v}{\partial \ln \varepsilon} \right)^{-1}$ relates the evolution of the specific surface with porosity. Concerning m , values of up to 10 have been reported, but usual values range between 1 and 2 [Tomadakis and Sotirchos(1993)]. Geometrical studies on classical porous media have shown that parameter n ranges between 1 and 2 ; so, the criterion for a full densification front is rarely met. However, for a large set of parameters, the residual open porosity in reactant depletion fronts is very low and may be safely neglected in the following.

The local front model relies on balance equations involving temperature (heat equation), precursor gas concentration (mass balance), and porosity (solid mass balance). These equations are written in a reference frame linked to the front, moving with a given velocity \mathbf{v} , and Cauchy data at hot and cold boundaries. The equations constitute then a nonlinear eigenvalue problem, which is solved by a shooting algorithm.

The results of the local front study are conveniently cast into the following relationships :

$$\begin{cases} v = \omega_f V_m C_c A k(T_h) \lambda_0 T_h^2 \frac{\mathcal{R}}{E_a q} \\ z_f = \xi_f \lambda_0 T_h^2 \frac{\mathcal{R}}{E_a q} \end{cases} \quad (3)$$

where ω_f and ξ_f are numbers close to unity which are respectively associated to scaled front velocity and front width, and the other symbols are explained in the list given in appendix.

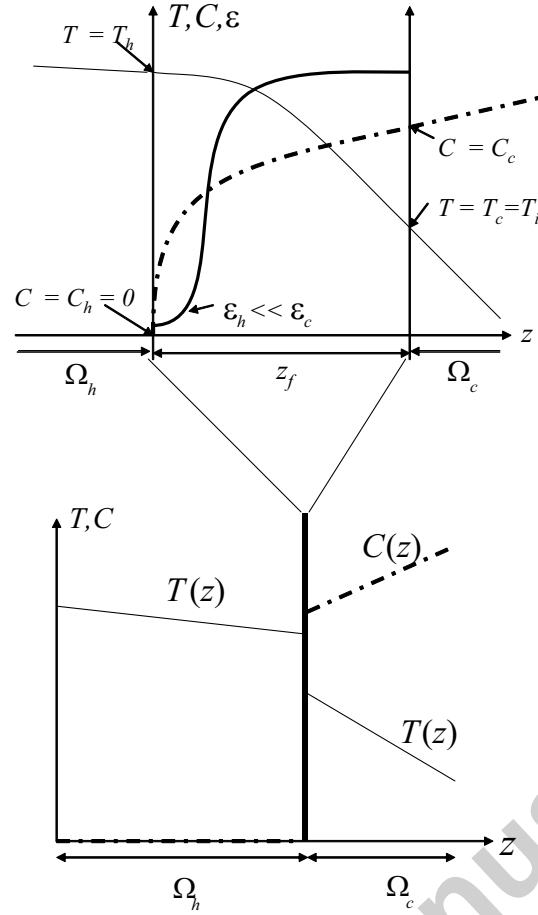


Fig. 2. Internal structure of an infiltration front in TG-CVI.

4 Global equations

If one now considers length scales much larger than the front width, the model may be represented as moving boundary problem, as usual in flame modelling. A solid surface recession problem has also been recently modelled in the same way [Duffa et al.(2005)].

Balance equations for heat and mass balance are required : they are defined in two domains : the raw, cold preform Ω_c and the hot, infiltrated preform Ω_h . It will be enough to consider that mass is transported only by diffusion and heat only by conduction. The transfer coefficients are functions of the local porosity; any effect of the local temperature will be neglected, since it would be of small magnitude compared to the effect of the activation energy on the reaction that takes place at the front. There are no source terms for heat

and mass outside the front; moreover, the transient times associated to heat and mass transfer have been proved to be short with respect to the reaction characteristic time. The heat and mass balance equations are consequently two Laplace equations, with domain-dependent coefficients :

$$\begin{cases} \operatorname{div}(-\lambda_c \nabla T) = 0 & \text{on } \Omega_c \\ \operatorname{div}(-\lambda_h \nabla T) = 0 & \text{on } \Omega_h \end{cases} \quad (4)$$

$$\begin{cases} \operatorname{div}(-D_c \nabla C) = 0 & \text{on } \Omega_c \\ C = 0 & \text{on } \Omega_h \end{cases} \quad (5)$$

The front will provide jump relations at the boundary. Fig. 2 summarizes the retained conditions. On the hot side, the temperature has a given value T_h , while on the cold side, it equals the ignition temperature T_i . Since the front is neither exo- nor endothermal, there is no jump in the heat flux \mathbf{q} , which is constant throughout the domain. However, since the thermal conductivity differs neatly from one side to the other, there will be a jump in thermal gradient :

$$\mathbf{q} = -\lambda_h \nabla T_h = -\lambda_c \nabla T_c \quad (6)$$

The mass flux \mathbf{J} arriving at the cold side is given by Fick's first law :

$$\mathbf{J} = -D_c \nabla C_c \quad (7)$$

As suggested by figure 3, let the front line be represented by the following equation :

$$S(x, z, t) = h(x, t) - z = 0 \quad (8)$$

In a reference frame moving with the front's velocity \mathbf{v} , this equation is conserved, so the Lagrangian derivative of S is zero, which yields :

$$\frac{\partial S}{\partial t} + \mathbf{v} \cdot \nabla S = 0 \quad (9)$$

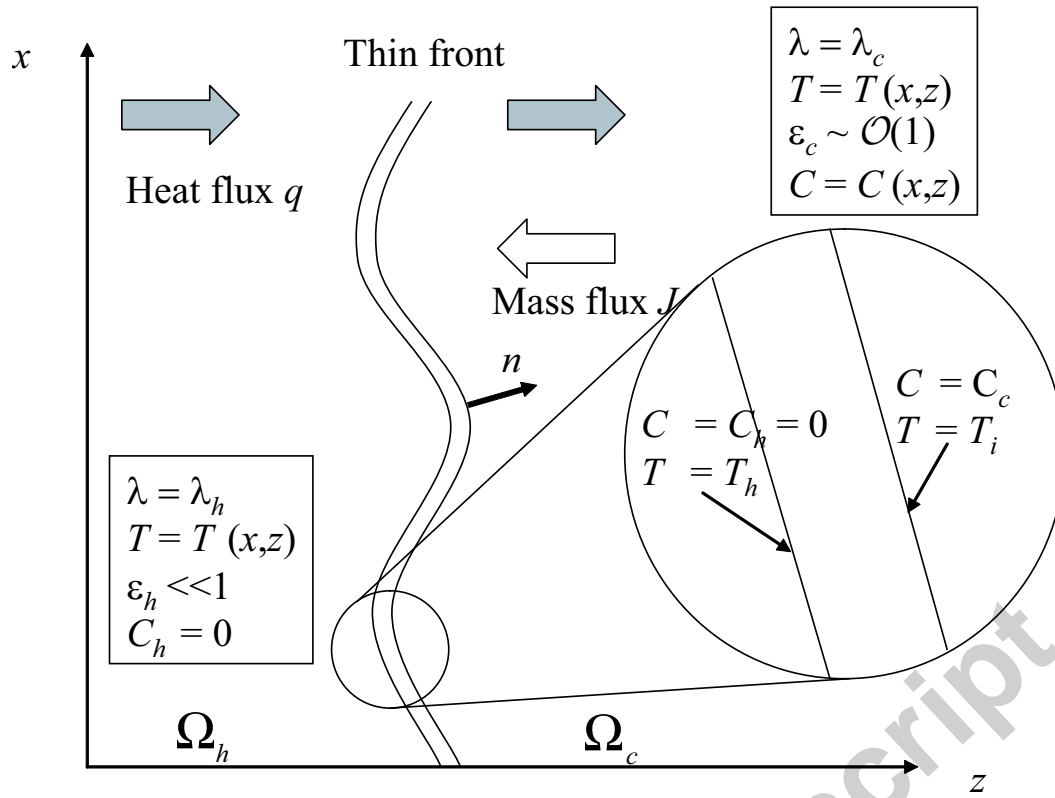


Fig. 3. Scheme for the 2D analysis of the front

The front velocity is oriented normal to the front line, the latter being defined by :

$$\mathbf{n} = \frac{\nabla S}{\|\nabla S\|} = \frac{1}{\sqrt{1 + \left(\frac{\partial h}{\partial x}\right)^2}} \begin{pmatrix} \frac{\partial h}{\partial x} \\ -1 \end{pmatrix} \quad (10)$$

The front velocity modulus is given by eq. 3. It is convenient to introduce an effective reaction rate :

$$R_{eff} = \omega_f Ak(T_h) \lambda_0 T_h^2 \frac{\mathcal{R}}{E_a |\mathbf{q} \cdot \mathbf{n}|} C_c \quad (11)$$

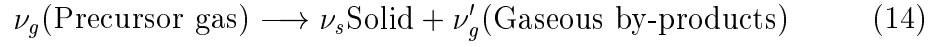
Consequently, the velocity vector becomes :

$$\mathbf{v} = V_m R_{eff} \mathbf{n} \quad (12)$$

Moreover, the reaction rate is also related to the mass flux through an interfacial mole balance :

$$R_{eff} = -\frac{\nu_s}{\nu_g} \mathbf{J} \cdot \mathbf{n} \quad (13)$$

where ν_s and ν_g are the stoichiometric coefficients involved in the heterogeneous reaction :



It will be convenient in the following to rewrite eq. 11 in a form which makes explicit its dependence on the cold-side concentration C_c and to the hot-side temperature T_h and thermal gradient ∇T_h :

$$R_{eff} = B \frac{k(T_h)}{|\nabla T_h \cdot \mathbf{n}|} C_c \quad (15)$$

where a pseudo-constant (*i. e.* it varies slowly with T_h) having the dimension of a thermal gradient, has been introduced :

$$B = \frac{\omega_f A T_h}{\gamma (1 - \varepsilon_r)} \quad (16)$$

Summarizing eqs. (9-13), a front propagation equation is given :

$$\frac{\partial h}{\partial t} = -\frac{\nu_s}{\nu_g} D V_m \left(\frac{\partial C}{\partial x} \frac{\partial h}{\partial x} - \frac{\partial C}{\partial z} \right) \quad \text{at } z = h(x, t) \quad (17)$$

The flux balance relation (13) may be developed as:

$$D_c \frac{\nu_s}{\nu_g} \left(\frac{\partial C}{\partial x} \frac{\partial h}{\partial x} - \frac{\partial C}{\partial z} \right) = B k(T_h) C_c \left| \frac{\partial T_h}{\partial x} \frac{\partial h}{\partial x} - \frac{\partial T_h}{\partial z} \right|^{-1} \left(1 + \frac{\partial h^2}{\partial x} \right) \quad \text{at } z = h(x, t) \quad (18)$$

Solutions of eqs. (4,5,17,18) will properly describe the front behavior.

5 Steady, plane solution

When considering a plane solution for the system (4,5,17,18), one should set $h(x) = \bar{h}$, *i.e.* as a constant in a coordinate frame following the front, moving at a constant velocity \mathbf{v} given by the result of the local study.

From Fick's first law and Fourier's law, and under the chosen hypotheses, it

is seen that concentration and temperature have piecewise linear profiles. For concentration, the solution is :

$$\left\{ \begin{array}{ll} \overline{C}(z) = C_c + \frac{\overline{J}}{D_c} (\overline{h} - z) & \text{in } \Omega_c \\ [C]_{z=\overline{h}} = C_c & \text{at } z = \overline{h} \\ \overline{C}_{z,c} = \frac{\partial \overline{C}}{\partial z} \Big|_{z=\overline{h}+0} = -\frac{\overline{J}}{D_c} & \text{at } z = \overline{h} + 0 \end{array} \right. \quad (19)$$

Similarly, for the temperature, the solution is :

$$\left\{ \begin{array}{ll} \overline{T}(z) = T_i + \frac{\overline{q}}{\lambda_c} (\overline{h} - z) & \text{in } \Omega_c \\ \overline{T}(z) = T_h - \frac{\overline{q}}{\lambda_h} (\overline{h} - z) & \text{in } \Omega_h \\ [\overline{T}] (z = \overline{h}) = T_i - T_h & \text{at } z = \overline{h} \\ \overline{T}_{z,c} = \frac{\partial \overline{T}}{\partial z} \Big|_{z=\overline{h}+0} = -\frac{\overline{q}}{\lambda_c} & \text{at } z = \overline{h} + 0 \\ \overline{T}_{z,h} = \frac{\partial \overline{T}}{\partial z} \Big|_{z=\overline{h}-0} = \frac{\overline{q}}{\lambda_h} & \text{at } z = \overline{h} - 0 \\ [\overline{T}_z] (z = \overline{h}) = -\overline{q} (\lambda_c^{-1} - \lambda_h^{-1}) & \text{at } z = \overline{h} \end{array} \right. \quad (20)$$

6 Linear perturbation analysis

Let (h, C, T) be a perturbation of position, concentration and temperature. The time evolution of these perturbations will be studied via a standard stability analysis. The method is similar to the one given in [Duffa et al.(2005)]. The following notations are introduced :

$$\left\{ \begin{array}{l} \Delta C = C - \overline{C} = \delta_C \exp(\omega_C t + k_{C,x}x + k_{C,z}z) \\ \Delta h = h - \overline{h} = \delta_h \exp(\omega_h t + k_{h,x}x) \\ \Delta T = T - \overline{T} = \delta_T \exp(\omega_T t + k_{T,x}x + k_{T,z}z) \end{array} \right. \quad (21)$$

where the ω_i and $k_{i,j}$ are possibly complex. Since the hot-side temperature will be of particular interest in the following, one will also introduce :

$$\Delta T_h = T_h - \overline{T}_h \quad (22)$$

In order to have a physically acceptable perturbation located at the front position , one should impose that $k_{C,z} \in \mathbb{R}^-$ and $k_{T,z} \in \mathbb{R}^-$ for $z \in \Omega_c$ and $k_{T,z} \in \mathbb{R}^+$ for $z \in \Omega_h$; this means that the perturbation amplitude is decreasing when z departs from \overline{h} and that it is not pseudo-periodic in the z direction. From the Laplace equations (4) and (5), the following relations arise :

$$\begin{cases} k_{T,x}^2 + k_{T,z}^2 = 0 \\ k_{C,x}^2 + k_{C,z}^2 = 0 \end{cases} \quad (23)$$

Consequently, the x -direction parameters :

$$\begin{cases} k_{T,x} = \pm j k_{T,z} \\ k_{C,x} = \pm j k_{C,z} \end{cases}, \quad (24)$$

are purely imaginary : this means that the perturbations are periodic in the transverse direction.

Introducing the perturbed solution in equation (17), and remembering that the unperturbed solution is flat (*i.e.* $\overline{h}_x = \overline{C}_x = 0$), one gets, up to first order in the perturbations, for $z = h$ and $\forall x, t$:

$$\omega_h \Delta h = -D_c V_m \frac{\nu_s}{\nu g} k_z \Delta C \quad (25)$$

This implies that Δh and ΔC have matching spatial periods along x :

$$\begin{cases} k_x = k_{h,x} = k_{C,x} \\ k_z = k_{C,z} \end{cases} \quad (26)$$

The coupling of the thermal perturbation to the other ones may only occur

through the mass balance relation valid at the front, eq. (18). This relation connects concentration at the cold side C_c only to the hot-side temperature and thermal gradient. However, since it is defined on the perturbed front, one has to perform the following developments :

$$\begin{aligned} C(z = h) &= \overline{C}(z = \overline{h}) + \overline{C}_z(z = \overline{h})\Delta h + \Delta C(z = \overline{h}) \\ T(z = h) &= \overline{T}(z = \overline{h}) + \overline{T}_z(z = \overline{h})\Delta h + \Delta T(z = \overline{h}) \end{aligned} \quad (27)$$

The result is the following relation :

$$\begin{aligned} -D_c \frac{\nu_s}{\nu_g} \left(k_z \overline{T}_{z,h} \Delta C + k_{T,z} \overline{C}_{z,h} \Delta T_h \right) = \dots \\ \dots Bk(\overline{T}_h) \left[\overline{C} \frac{\partial \ln k}{\partial T} (\Delta T_h + \overline{T}_{z,h} \Delta h) + \Delta C + \overline{C}_z \Delta h \right] \end{aligned} \quad (28)$$

where all quantities are evaluated at $z = \overline{h}$. Equation (28) suggests that the temperature perturbation has the same space period as the concentration and height. As a consequence, $k_{T,z} = k_z$. There are now two relationships involving ω_h and k_z , as needed, but there are three perturbations present instead of two; so, one needs a third relationship in order to provide the necessary closure. A thermal balance will be of little interest, since the front is considered athermal. Fortunately, a simple and reasonable assumption may be performed. Considering a front with constant width, the jump relationship for T is preserved through the perturbed front : this implies that T_h is a constant at all points of the perturbed front, since $T_c = T_i$ by definition on the cold side. The perturbed temperature field in Ω_h is schematized at figure 4. This assumption may be safe as long as one deals with length scales much superior to the front thickness; in accordance, curvature effects on the front characteristic quantities may also be discarded.

Then, up to first order, the last two terms in the temperature development

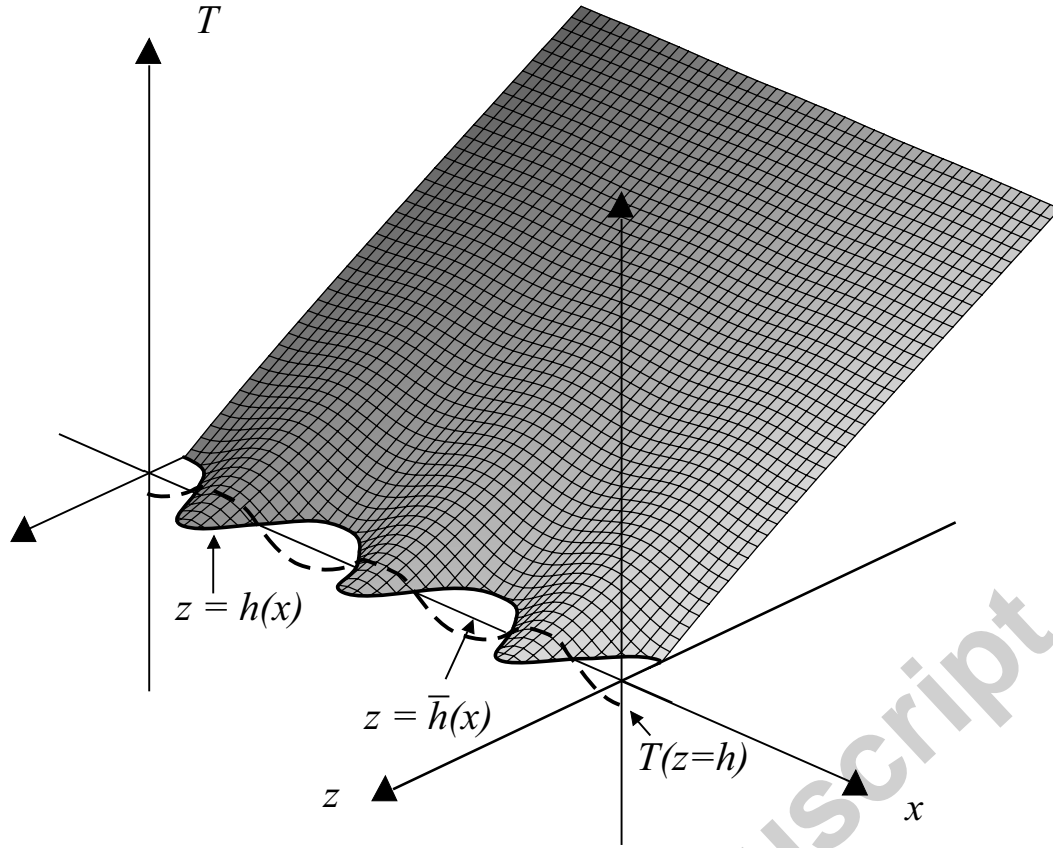


Fig. 4. Scheme of a temperature perturbation following the front's perturbed position

(27) cancel out each other :

$$\Delta T_h(z = \bar{h}) \approx -\Delta h \bar{T}_{z,h}(z = \bar{h}) \quad (29)$$

Inserted in eq. (28), this approximation gives :

$$-\Delta C \left(D_c \frac{\nu_s}{\nu_g} k_z + \frac{Bk(\bar{T}_h)}{\bar{T}_{z,h}} \right) = \Delta h \left(\frac{Bk(\bar{T}_h)}{\bar{T}_{z,h}} + D_c \frac{\nu_s}{\nu_g} k_z \bar{C}_z \right) \quad (30)$$

Combined to eq. (25), this relation is sufficient to obtain a dispersion relation, by eliminating ΔC and Δh . The results are presented and discussed in the next section.

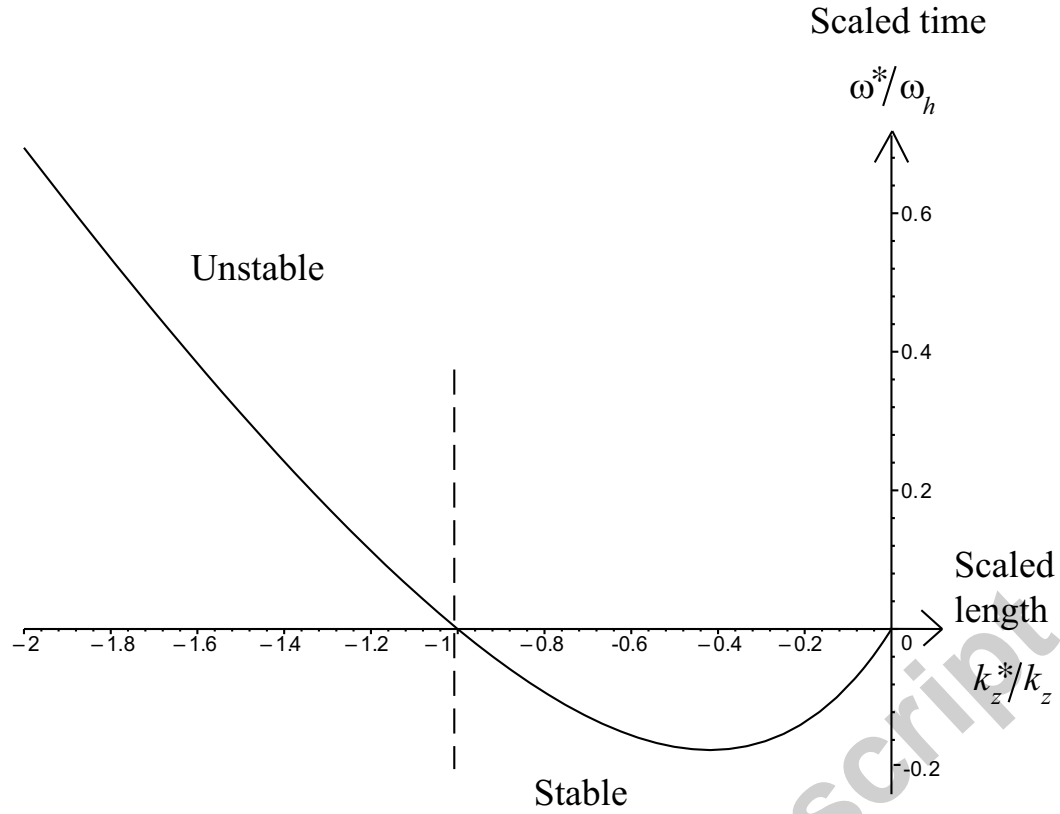


Fig. 5. Plot of the dispersion relation in scaled length and time coordinates

7 Results and discussion

Solving the linear system in $(\Delta h, \Delta C)$ formed by eqs. (25,30) yields finally the dispersion relation :

$$\omega_h = \omega^* \frac{\frac{k_z}{k_z^*} - K}{\frac{k_z}{k_z^*} + 1} \quad (31)$$

Figure 5 is a plot of eq. (31). It shows that for decay lengths inferior to the critical length $(k_z^*)^{-1}$, then the perturbations are damped out; on the other hand, if they are broader, they can be amplified. However, for very large decay lengths, the amplification time is extremely long, which means that the instability does not have a chance to grow before the infiltration process is completed.

In eq. (31), three characteristic quantities have appeared :

- A characteristic decay inverse length :

$$k_z^* = \frac{\omega_f Ak(T_h) \cdot L_{ref}}{D_c |\frac{\nu_s}{\nu_g}|}.$$

- A characteristic decay time :

$$\omega^* = (C_c V_m) \frac{(\omega_f Ak(T_h) \cdot L_{ref})^2}{D_c |\frac{\nu_s}{\nu_g}|}$$

- A dimensionless constant :

$$K = \frac{\overline{C}_z}{k_z^* C_c}.$$

Remembering that in the low-velocity limit [Nadeau et al.(2006)], $\overline{J} = D_c \overline{C}_z \simeq C_c Ak(T_h) L_{ref} \cdot \varepsilon_c \omega_f$, one has actually $K \simeq \varepsilon_c$.

The reference length appearing in these relations is the natural scaling for the front width [Nadeau et al.(2006)]:

$$L_{ref} = \frac{\lambda_0 \mathcal{R} T_h^2}{E_a \overline{q}} = z_f / \xi_f \quad (32)$$

Note that the ratio of the front length to the critical inverse length is proportional to a squared Thiele modulus :

$$\frac{L_{ref}}{(k_z^*)^{-1}} = \omega_f L_{ref}^2 \frac{Ak(T_h)}{D_c |\frac{\nu_s}{\nu_g}|} = \omega_f \Phi^2. \quad (33)$$

It has been shown [Vignoles et al.(2005)] that this Thiele modulus is also the ratio between a critical heat flux q^* , necessary for the front to exist, and the actual flux \overline{q} . Eq. (33) may be written in a more convenient form :

$$k_z^* = \frac{\omega}{L_{ref}} \left(\frac{\overline{q}}{q^*} \right)^2 \quad (34)$$

Choosing a flux 3 times larger than the minimal required value gives a decay length (and transverse wavelength) 39 times larger than the front thickness, which validates the scope of the model.

The characteristic time scale for the process is [Nadeau et al.(2006)]:

$$\tau = (C_c V_m Ak(T_h))^{-1} \quad (35)$$

The characteristic inverse time may then be recast into the following form :

$$\omega^* = \frac{\omega_f^2}{\tau} \left(\frac{\bar{q}}{q^*} \right) \quad (36)$$

This quantity is less sensitive to the heat flux than k_z^* . Moreover, it has a strong dependence on temperature and initial pore diameter, because A scales as the inverse of this parameter [Nadeau et al.(2006)].

Numerical evaluation has been performed with data that have been used in the previous works which have allowed one to validate the modelling approach [Vignoles et al.(2006), Nadeau et al.(2006)], provided at tables 1 and 2. The ratio of the decay/growth times to the total processing times is plotted at figure 6 : it ranges from unity for the lowest temperatures ($800^\circ C$) to small values ($\approx 5 \cdot 10^{-3}$) for the highest ones ($1300^\circ C$), showing that the dynamical behavior of the front is fully expressed throughout the infiltration run only for large enough temperatures (*i.e.* $> 1000^\circ C$).

These results show indeed that the infiltration front is not unconditionally stable; the practical consequence is that undesired infiltrations may occur. Fortunately, this is rarely the case, since the processing conditions are such that :

- the processing temperatures are mild, so that the characteristic growth time is not too small;
- the characteristic perturbation dimensions are larger or comparable to the whole sample transverse length.

However, scaling up the process could lead to more pronounced problems. The expressions given for the critical length and time may then help to avoid them, by giving constraints for a safe infiltration. For instance, it may be readily seen from eqs. (35-36) that decreasing the initial pore diameter (*i.e.* increasing A) would decrease the perturbation growth time : a preform with thinner or more

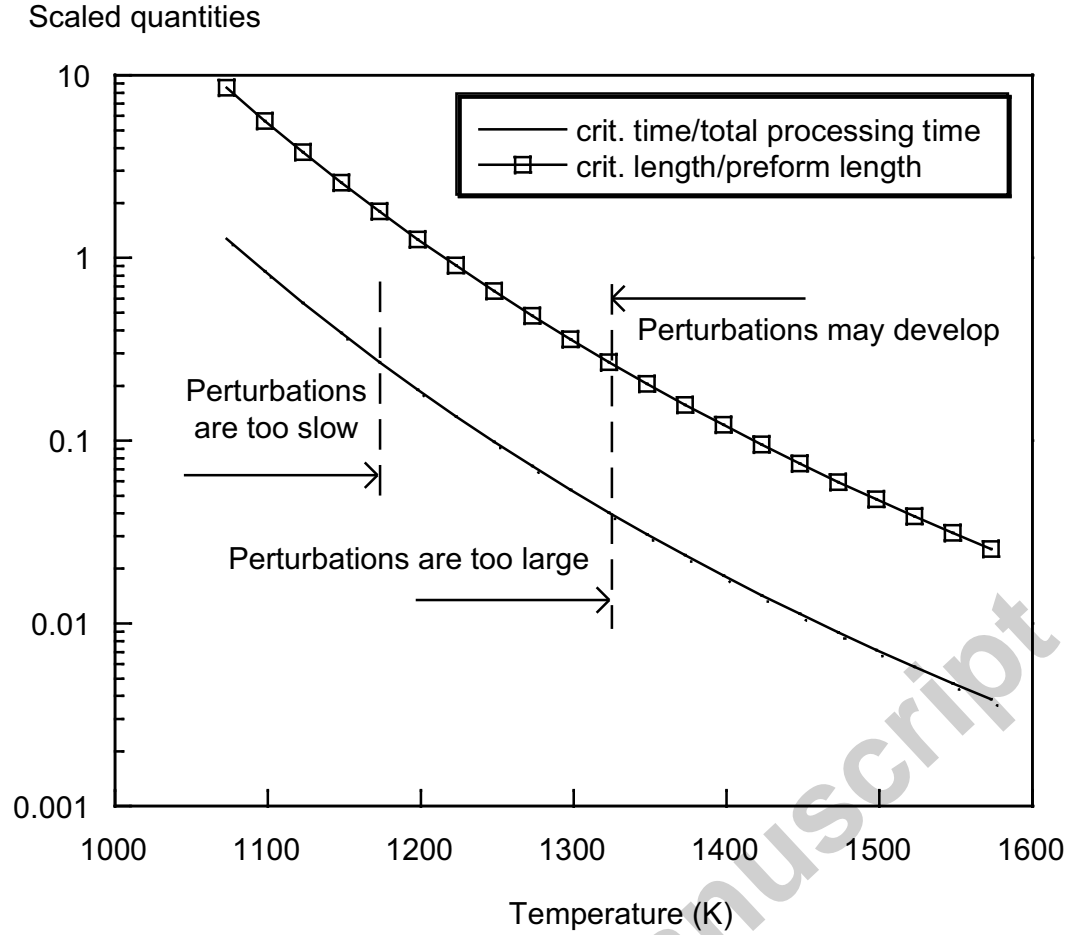


Fig. 6. Temperature plots of *i*) Perturbation growth time compared to the total processing time as a function of temperature (continuous line), and *ii*) Critical length compared to the preform length (squares).
closely packed fibers would be more sensitive to front perturbations.

8 Conclusion

A standard analytical stability study has been performed on a previously validated TG-CVI/Film-boiling quasi-analytical model. The approach followed here has consisted in:

- Writing down a propagation equation for the front in 2D.
- Introducing perturbations of the system on the front geometry, concentration and temperature. The perturbations of the three variables are shown to

be intimately connected to each other : they share the same characteristic space and time period.

A conditional stability arises : there is a range of wave numbers for which the system becomes unstable, below a critical value, which is directly linked to the ratio of the provided heat flux to the minimal required heat flux, necessary for the front to exist. The characteristic time for perturbation growth is large when the processing temperature is moderate enough; however, for high temperatures, or for large preform dimensions, perturbations are prone to show up and deteriorate the final part quality. In some way, this study shows that engineers developing the process have had some luck, since there is a possibility for unstable behavior, which is rarely achieved in practice; however, some unexplained failed experiments could be analyzed using the results of this work.

Acknowledgments

The authors acknowledge N. Nadeau (MAB, University Bordeaux 1) and C. Robin-Brosse (Snecma Propulsion Solide) for helpful discussions.

References

- [Besmann and McLaughlin(1994)] Besmann, T. M., McLaughlin, J. C., 1994. Scale up and modeling of forced CVI. In: Logan, K. V. (Ed.), Proceedings of the 18th Annual conference on Composites and Advanced Materials - B. Vol. 15. The American Ceramic Society, Westerville, OH, pp. 897–907.
- [Besmann et al.(1991)] Besmann, T. M., Sheldon, B. W., Lowden, R. A., Stinton, D. P., 1991. Vapor-phase fabrication and properties of continuous-filament ceramic composites. *Science* 253, 1104–1109.

- [Bruneton et al.(1997)] Bruneton, E., Narcy, B., Oberlin, A., 1997. Carbon-carbon composites prepared by a rapid densification process. *Carbon* 35 (10-11), 1593–1611.
- [Chung et al.(1991)] Chung, G. Y., McCoy, B. J., Smith, J. M., 1991. Chemical vapor infiltration - Modelling solid matrix deposition in ceramic-matrix composites. *Chem. Eng. Sci.* 46, 723–734.
- [Devlin et al.(1996)] Devlin, D. J., Barbero, R. S., Siebein, K. N., 1996. Radio frequency assisted chemical vapor infiltration. In: Allendorf, M. D., Robinson, M., Ulrich, R. K. (Eds.), *Chemical Vapor Deposition XIII*. Vol. PV 96-5 of The Electrochemical Society Proceedings Series. The Electrochemical Society, The Electrochemical Society, Pennington, NJ, pp. 571–577.
- [Devlin et al.(1992)] Devlin, D. J., Currier, R. P., Barbero, R. S., Espinoza, B. F., 1992. Microwave assisted chemical vapor infiltration. In: Besmann, T. M., Gallois, B. M., Warren, J. W. (Eds.), *Chemical Vapor Deposition of Refractory Metals and Ceramics II*. Vol. 250 of Mater. Res. Soc. Symp. Proc. Materials Research Society, Pittsburgh, Pennsylvania, pp. 245–250.
- [Duffa et al.(2005)] Duffa, G., Vignoles, G. L., Goyh  n  che, J.-M., Aspa, Y., 2005. Ablation of carbon-based materials : investigation of roughness set-up from heterogeneous reactions. *Int. J. of Heat and Mass Transfer* 48, 3387–3401.
- [F  dou et al.(1993)] F  dou, R., Langlais, F., Naslain, R., 1993. A model for the isothermal isobaric CVI in a straight cylindrical pore. Application to the CVI of SiC. *J. of Mater. Synth. and Process.* 1 (2), 61–74.
- [Golecki(1997)] Golecki, I., 1997. Rapid vapor-phase densification of refractory composites. *Mater. Sci. Eng. R20*, 37–124.
- [Golecki et al.(1994)] Golecki, I., Morris, C., Narasimhan, D., 1994. US Patent no. 5 348 774.
- [Gupta and Evans(1991)] Gupta, D., Evans, J. W., 1991. A mathematical model for CVI with microwave heating and external cooling. *J. Mater. Res.* 6, 810–818.

- [Gupte and Tsamopoulos(1989)] Gupte, S. M., Tsamopoulos, J. A., 1989. Densification of porous materials by chemical vapor infiltration. J. Electrochem. Soc. 136, 555.
- [Houdayer et al.(1984)] Houdayer, M., Spitz, J., Tran Van, D., 1984. US Patent no. 4 472 454.
- [Leutard et al.(2002)] Leutard, D., Vignoles, G. L., Lamouroux, F., Bernard, B., 2002. Monitoring density and temperature in *C/C* composites elaborated by CVI with radio-frequency heating. J. Mater. Synth. and Proc. 9 (5), 259–273.
- [Lines et al.(2005)] Lines, J.-F., Vignoles, G. L., Goyh  n  che, J.-M., Puiggali, J.-R., 2005. Thermal modelling of a carbon/carbon composite material fabrication. In: Denis, S. (Ed.), Proc. Intl. Conf. on Thermal Process Modelling and Computer Simulation 2003. Vol. 120 of J. Phys. IV France. EDP Sciences, Les Ulis, France, pp. 291–297.
- [Melkote and Jensen(1990)] Melkote, R. R., Jensen, K. F., 1990. A model for chemical vapor infiltration of fibrous substrates. In: Besmann, T. M., Gallois, B. M. (Eds.), Chemical Vapor Deposition of Refractory Metals and Ceramics. Vol. 168 of Mat. Res. Soc. Symp. Proc. Materials research Society, Pittsburgh, Pennsylvania, pp. 67–72.
- [Middleman(1989)] Middleman, S., 1989. The interaction of chemical kinetics and diffusion in the dynamics of chemical vapor infiltration. J. Mater. Res. 4, 1515–1524.
- [Midha and Economou(1997)] Midha, V., Economou, D. J., 1997. A two-dimensional model of chemical vapor infiltration with radio frequency heating. J. Electrochem. Soc. 144, 4062–4071.
- [Morell et al.(1992)] Morell, J. I., Economou, D. J., Amundson, N. R., 1992. Pulsed-power volume-heating chemical vapor infiltration. J. Mater. Res. 7, 2447–2457.
- [Nadeau et al.(2006)] Nadeau, N., Vignoles, G. L., Brauner, C.-M., 2006. Analytical and numerical study of the densification of carbon/carbon composites by a film-boiling chemical vapor infiltration process. Chem. Eng. Sci 61, 7509–7527.

- [Naslain and Langlais(1990)] Naslain, R., Langlais, F., 1990. Fundamental and practical aspects of the chemical vapor infiltration of porous substrates. High Temperature Science 27, 221–235.
- [Reuge and Vignoles(2005)] Reuge, N., Vignoles, G. L., 2005. Global modelling of I-CVI : Effects of reactor control parameters on a densification. J. Mater. Process. Technol. 166, 15–29.
- [Sotirchos(1991)] Sotirchos, S. V., 1991. Dynamic modelling of chemical vapor infiltration. AIChE J. 37, 1365–1382.
- [Starr et al.(1991)] Starr, T. L., Smith, A. W., Vinyard, G. F., 1991. Model assisted control of CVI for ceramic fabrication. Ceram. Eng. Sci. Proc. 12, 2017.
- [Tomadakis and Sotirchos(1993)] Tomadakis, M. M., Sotirchos, S. V., 1993. Ordinary, transition and Knudsen regime diffusion in random capillary structures. Chem. Eng. Sci. 48 (19), 3323–3333.
- [Vaidyaraman et al.(1995)] Vaidyaraman, S., Lackey, W. J., Freeman, G. B., Agrawal, P. K., Langman, M. D., 1995. Fabrication of carbon-carbon composites by forced flow-thermal gradient chemical vapor infiltration. J. Mater. Res. 10 (6), 1469–1477.
- [Vignoles et al.(2006)] Vignoles, G. L., Goyh  n  che, J.-M., S  bastian, P., Puiggali, J.-R., Lines, J.-F., Lachaud, J., Delha  s, P., Trinqu  coste, M., 2006. The film-boiling densification process for *C/C* composite fabrication : From local scale to overall optimization. Chem. Eng. Sci. 61, 5336–5353.
- [Vignoles et al.(2005)] Vignoles, G. L., Nadeau, N., Brauner, C.-M., Lines, J.-F., Puiggali, J.-R., 2005. The notion of densification front in CVI processing with temperature gradients. In: E. Lara-Curzio, D. Z., Kriven, W. M. (Eds.), Mechanical Properties and Performance of Engineering Ceramics and Composites. Vol. 26 of Ceramic Engineering and Science Proceedings. The American Ceramic Society, Westerville, OH, pp. 187–195.

List of symbols

Latin

Symbol	Definition and unit
A	Internal surface area scale factor, m^{-1}
B	Auxiliary variable, see eq. (16), $K.m^{-1}$
C	Gaseous precursor concentration, $mol.m^{-3}$
D	Diffusion coefficient, $m^2.s^{-1}$
h	Position of the front, m
J	Mole flux, $mol.m^{-2}.s^{-1}$
L	length, m
m	Archie's law exponent (-)
n	surface area variation exponent (-)
p	total pressure, Pa
q	heat flux, $W.m^{-2}.K^{-1}$
\mathcal{R}	perfect gas constant, $J.mol^{-1}.K^{-1}$
R	precursor consumption rate, $mol.m^{-3}.s^{-1}$

Latin (cont'd)

Symbol	Definition and unit
t	time, s
T	temperature, K
V_m	deposit molar volume, $m^3.mol^{-1}$
\mathbf{v}	front velocity, $m.s^{-1}$
x	space coordinate, m
z	space coordinate, m

Greek

Symbol	Definition and unit
α	reaction rate order (-)
γ	dimensionless activation energy (-)
ε	porosity (-)
λ	thermal conductivity, $W.m^{-1}.K^{-1}$
ξ	scaled space coordinate(-)
σ_v	internal surface area, m^{-1}
τ	characteristic time, s
Φ	Thiele modulus (-)
ω	dimensionless front velocity (-)

Subscripts and underscripts

Symbol	Definition and unit
\cdot_0	refers to initial state (raw material, pure gas, ...)
\cdot_c	refers to the cold side of the front
\cdot_f	refers to the front
\cdot_g	gas
\cdot_h	refers to the hot side of the front
\cdot_i	ignition
\cdot_{eff}	effective value
\cdot_{lim}	limiting value
\cdot_{ref}	reference value
\cdot_t	total

Symbol	Meaning	Expression	Value/Unit
ε	Porosity		
	Initial porosity on the cold side	$\varepsilon_c = \varepsilon_0$	0.94
	Residual, closed porosity on the hot side	$\varepsilon_h = \varepsilon_r$	0.04
λ	Thermal conductivity	$(1 - \varepsilon)\lambda_0$	
	Solid phase thermal conductivity	λ_0	$8.2 \text{ W.m}^{-1}.\text{K}^{-1}$
	Hot side thermal conductivity	$\lambda_h = \lambda_0 (1 - \varepsilon_r)$	$7.87 \text{ W.m}^{-1}.\text{K}^{-1}$
	Cold side thermal conductivity	$\lambda_c = \lambda_0 (1 - \varepsilon_c)$	$0.49 \text{ W.m}^{-1}.\text{K}^{-1}$
V_m	Deposit molar volume	$\frac{M_s}{\rho_s}$	$6.0 \cdot 10^{-6} \text{ m}^3.\text{mol}^{-1}$
D	Effective gas diffusivity	$D_0 \varepsilon^{m+1}$	
	Pure gas diffusion coefficient	D_0	$9 \cdot 10^{-5} \text{ m}^2.\text{s}^{-1}$
	Archie's law exponent	m	2
	Cold side diffusion coefficient	$D_c = D_0 \varepsilon_c^{m+1}$	$7.5 \cdot 10^{-5} \text{ m}^2.\text{s}^{-1}$
σ_v	Internal surface area	$A \varepsilon^{1/n} (1 - B\varepsilon)$	
	Parameters	A	$4.0 \cdot 10^5 \text{ m}^{-1}$
		B	1/2
		n	2
k	Chemical deposition rate constant	$k_0 \exp(-\frac{E_a}{RT})$	
	Kinetic constant	k_0	$1.1 \cdot 10^8 \text{ m.s}^{-1}$
	Activation energy	E_a	$3.26 \cdot 10^5 \text{ J.mol}^{-1}$

Table 1
List of provided parameter laws and values

Symbol	Meaning	Expression	Value/Unit
T_h	Hot-side temperature		1073 — 1573 K
T_i	Ignition temperature		1000 K
p	Total pressure		$1.015 \cdot 10^5 \text{ Pa}$
C_c	Cold-side concentration	$p/\mathcal{R}T_i$	12.2 mol.m^{-3}
$\frac{\nu_g}{\nu_s}$	Stoichiometric ratio		-1.29
q^*	Critical heat flux	$q^* = L_{ref}^{-1} \sqrt{\frac{D_0 \nu_s/\nu_g }{Ak(T_h)}}$	$W.m^{-2}$
\bar{q}	Heat flux	$\bar{q} = 3q^*$	$W.m^{-2}$
L_t	Preform width		15 cm
t_t	Total infiltration time	$t_t = L_t/v_f$	s

Table 2

List of provided values for numerical evaluations

List of Figures

1	Descriptive scheme of the film-boiling CVI process.	7
2	Internal structure of an infiltration front in TG-CVI.	9
3	Scheme for the 2D analysis of the front	11
4	Scheme of a temperature perturbation following the front's perturbed position	16
5	Plot of the dispersion relation in scaled length and time coordinates	17
6	Temperature plots of <i>i</i>) Perturbation growth time compared to the total processing time as a function of temperature (continuous line), and <i>ii</i>) Critical length compared to the preform length (squares).	20

List of Tables

1	List of provided parameter laws and values	29
2	List of provided values for numerical evaluations	30